Mier, J.A., Sánchez, R., & Newman, D. E. 2020. Tracer particle transport dynamics in the diffusive sandpile cellular automaton. *In Chaos, Solitons & Fractals, 140*, 110117-110126

DOI:10.1016/j.chaos.2020.110117.

Tracer particle transport dynamics in the diffusive sandpile cellular automaton

J. A. Mier[1*], R. Sanchez[2] and D. E. Newman[3]
[1]*Departamento de Física Aplicada, Universidad de Cantabria, 39005 Santander, Spain*
[2]*Departamento de Física, Universidad Carlos III de Madrid, 28911 Leganés, Madrid, Spain*
[3]*Department of Physics, University of Alaska, Fairbanks, AK 99775-5920, USA*
(Dated: July 18, 2019)

The confinement properties of the diffusive running sandpile are characterized by tracking the motion of a population of marked grains of sand. It is found that, as the relative strength of the avalanching and diffusive transport channels is varied, a point is reached at which the particle global confinement time and the probability density functions of the jump-sizes and waiting-times of the tracked grains experience a sudden change, thus revealing a dynamical transition, consistently with previous studies [D. E. Newman *et al.*, Phys. Rev. Lett. **88**, 204304 (2002)]. Across the transition, the sandpile moves from a regime characterized by self-similarity and memory, where avalanches of all possible sizes dominate transport across the system, to another regime where transport is taken over by near system-size, quasi-periodic avalanches. Best values for the fractional transport exponents that quantify the effective transport across the sandpile prior to the transition are also obtained.

I. INTRODUCTION

Many studies have relied on the concept of self-organized criticality[1] (SOC) as a possible explanation of the overall dynamics of a wide variety of physical and biological systems[2–9]. All of them justify this hypothesis by the presence of many of the basic ingredients for SOC dynamics. Namely, an open driven system with a local instability threshold that generates local transport when overcome, and a large disparity between the temporal scales associated to the drive and the instability relaxation. It is not difficult to find systems that fit into this type of description, at least in an approximate manner. The transport processes in them, often dominated by avalanching processes, is intrinsically bursty and of a non-diffusive nature. At steady state conditions, SOC systems exhibit properties such as spatial self-similarity, temporal persistence (memory effects) and long-term correlations, that are typical from critical points. However, these properties appear here without any need for fine-tuning, in contrast to equilibrium critical points. That is why the dynamics are known as self-organized criticality.

The running sandpile automaton[10,11] embodies many of the features that one often associates with SOC. It appeared simultaneously with the proposal of self-organized criticality, providing a simple paradigm to illustrate SOC dynamics. Many versions of the sandpile have appeared over the years, each tailored to specific applications. Of particular interest to us is the so-called diffusive running sandpile[12] that was first formulated in the context of magnetically confined fusion plasmas with the purpose of understanding the dynamics of radial transport in situations where near-marginal turbulence coexisted with other types of (diffusive) transport in tokamak plasmas[13]. The transport characteristics of the diffusive sandpile have been characterized in a number of ways over the years[14–16]. Its most remarkable features are that: 1) SOC features are maintained for finite, albeit small, strengths of the diffusive channel relative to the avalanche channel and 2) that, at larger values of their relative strength, a sudden transition takes place in which transport is no longer dominated by SOC-like avalanches, but by near-system wide global discharge events. It has also been shown that is possible to characterise this dynamical transition across many sandpile runs in terms of a single parameter that essentially measures the average roughness of the sandpile profile allowed by the transport taking place in the system[14].

In this paper we further inquire into the nature of transport in the diffusive running sandpile cellular automaton by following and analyzing the motion of a selected group of marked (or tracer) particles. Their trajectories are used to calculate the average particle confinement time as well as their jump-size and waiting-time probability density functions (pdfs). It will be shown that the dynamics that are known to dominate both prior and after the transition can be well captured and uniquely quantified by these diagnostics. Furthermore, we will also use the tracer information to construct a suitable effective transport model based on fractional transport equations[17] for both dynamical regimes, and to estimate the optimal values of the transport exponents that define this model.

The paper is thus organized as follows. First, the diffusive sandpile is reviewed in Sec. II . Then, in Sec. III, the rules that govern the motion of the marked particles are presented and discussed. These rules are rather subtle since there is a certain freedom to specify them since the diffusive sandpile dynamics do not distinguish between individual grains. Next, the main results of the paper regarding tracked particle motion will be discussed in Secs. IV and V and an effective model for transport

*Corresponding author: mierja@unican.es

is built for the diffusive sandpile. The model equation contains both fractional derivatives in space and time, and the corresponding fractional exponents are quantified numerically. Finally, some conclusions will be drawn in Sec. VI.

II. THE DIFFUSIVE SANDPILE MODEL

The diffusive sandpile[12] is an extension of the standard one-dimensional running sandpile that contains an additional diffusive transport channel whose intensity can be tuned relative to the avalanche-like one. The sandpile domain consists of L cells or sites, numbered from $x = 1$ to $x = L$ (i.e., $x = 1, 2, \ldots, L-1, L$ are the allowed values). A variable $h(x)$ is assigned to each radial location x, that represents the height of sand at that site. The temporal evolution of the sandpile is performed by randomly adding, at each iteration, a grain of sand to every cell with probability P_0. The critical character of the sandpile dynamics is introduced by a critical slope value, $-Z_c$, $Z_c > 0$. Whenever the local slope, $Z(x) = h(x+1) - h(x)$, exceeds this threshold, N_f grains of sand are moved from the unstable cell to the next one. All sandpile cells are checked for instability once per iteration.

Diffusive transport is introduced by adding a local net diffusive flux, Γ_d, that is given at each cell by $\Gamma_d(x) = -D_0\,[Z(x-1) - Z(x)] = \Gamma_d^+(x) - \Gamma_d^-(x)$. Here, D_0 is the diffusion coefficient. The net flux at cell x is thus simply the difference of the amount of sand reaching the cell diffusively from the previous cell at $x-1$, $\Gamma_d^+(x) = -D_0 Z(x-1)$, and the amount of sand leaving that cell diffusively to the next cell at $x+1$, $\Gamma_d^-(x) = -D_0 Z(x)$. This rule is just a discretized version of the classical diffusive term $D_0 d^2h/dx^2$ (i.e. $h(x) = h(x) + D_0\,[h(x+1) - 2h(x) + h(x-1)]$).

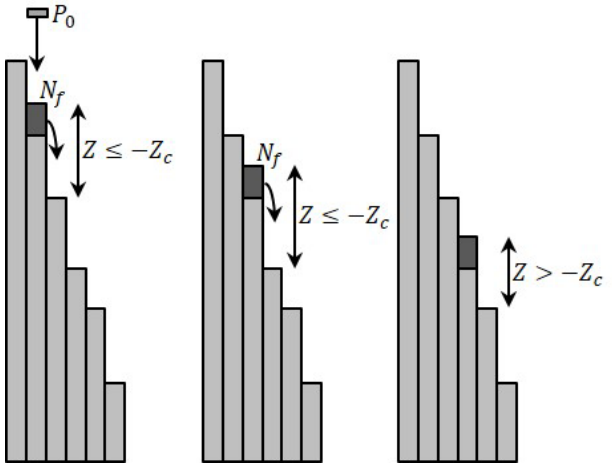

FIG. 1: Diagram explaining the one-dimensional diffusive sandpile automaton rules. Unlike the classical (non-diffusive) sandpile, a diffusive flux is incorporated to each cell now (see in the text for more details).

Finally, the sandpile has a closed boundary at $x = 1$ (no particles enter that cell from the left), and an open boundary condition at $x = L$ (particles reaching that cell are removed). The condition $N_f > P_0 L - D_0 Z_a$ has to be fulfilled in order to avoid the sandpile become overdriven. Here, $Z_a = Z_c - N_f/2$ is the average value[18] of the slope at the bottom edge cell, $x = L$.

Under a steady external drive (throughout this paper, $P_0 \in [10^{-4} - 10^{-3}]$ has been used), the diffusive sandpile eventually reaches a steady state in which the incoming sand will balance (on average) the edge outflux. The diffusive sandpile domain will be split into two regions connected at the intermediate cell $x_t = D_0(Z_c - N_f)/P_0$. In the region to the left of x_t the slope is well below $-Z_c$. Therefore, transport will be entirely carried out through the diffusive channel. In the region to the right of x_t, transport will be driven by both diffusive and avalanche channels. The value of x_t is estimated by locating the outermost position at which the integrated source ($P_0 x_t$) can still be entirely removed by diffusion while keeping the gradient below the minimum value accessed during avalanche activity in the SOC steady state (i.e., $Z(x_t) < Z_c - N_f$). The analytical values provided for both Z_a and x_t agree well with those obtained from simulations.

III. ADVANCING TRACERS IN THE DIFFUSIVE SANDPILE

In this work all marked sand grains will be advanced together with the rest of the sand in the sandpile, but they are treated differently in the sense that each tracer is transparent, not being taken into account when a cell is checked for instability or when updating the local sandpile height.

Since the diffusive sandpile dynamics are formulated in such a way that individual grains are not evolved separately, the trajectory of a single tracer particle can in principle be defined in various ways (that depend on the kind of underlying dynamics we are interested in), with the only restriction of them being compatible with the sandpile governing rules. Here, we have examined one approach that assumes that **only** those particles that are within the **active surface strip** of depth N_f at each cell (see dark grey regions in Fig. 2(b)) can move to the next cell as a result of an avalanche or diffusion. That is, if an avalanche happens and N_f grains must be moved to the next cell, they will necessarily be the ones closer to the surface of the cell. This situation is closer to what takes place in a real sandpile, where only the grains closer to the surface are transported down the slope, whilst those which are more deeply buried stay at rest for very long times. However, it is interesting to note that other set of rules might be more appropriate for other systems. One could, for instance, assume that **any** tracked particle at a particular cell (see dark grey regions in Fig. 2(a)) can move to the next cell as a result of an avalanche or of

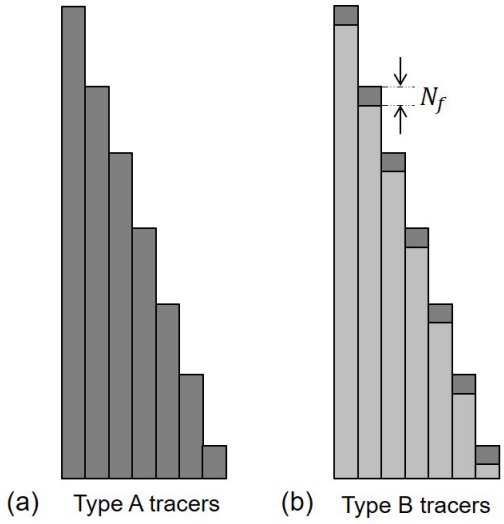

FIG. 2: Sketch showing the active tracer regions of the two formulations discussed in text. In (a), particles can be anywhere in the cell. In (b), particles are confined in the top N_f positions in the cell. The dark grey regions represent the possible locations of tracked particles for both cases.

diffusive transport, **independently** of its relative depth within that cell. That is, if an avalanche happens and N_f grains must be moved to the next cell, the grains that are moved will be chosen from within those inside the cell with equal probability. We will not examine this case in this paper, though.

Trajectories for Tracked Particles

We proceed next to define exactly how tracers will be advanced in this work. Each of the marked grains will be labeled using the superindex m, and will be positioned at some initial time, t_0^m, at an arbitrary cell, x_0^m, chosen randomly from within a small subset of prescribed cells close to the top of the pile. Within that cell, their depth, as measured from the top, will be set to $d_0^m = uN_f$, where u is a random number uniformly distributed in $[0, 1]$. As the sandpile evolves, the position, x^m, and depth, d^m of each marked grain of sand will change once the drive has been completed and stability for each cell checked. The position of each marked grain at the k-th iteration is again updated in two steps. Secondly, and just after the computation of the diffusive term, its action on the tracers is considered. The specific rules that govern this process are thus as follows:

I) **Avalanche transport channel**[18,19]:

(1) If the current cell is stable ($Z > -Z_c$) and no grains of sand have been added during the driving phase, the tracer remains at the same cell,
$x^m(k) = x^m(k-1)$,
and its depth remains unchanged,
$d^m(k) = d^m(k-1)$.

(2) If the current cell is stable but one grain of sand has been dropped on it in the driving phase, the tracer remains in the same cell,
$x^m(k) = x^m(k-1)$,
and its depth is increased by one,
$d^m(k) = d^m(k-1) + 1$.

(3) If the current cell is stable, but the previous one is unstable and moves N_f grains over the current cell, the tracer remains in the same cell,
$x^m(k) = x^m(k-1)$,
and its depth is increased by N_f,
$d^m(k) = d^m(k-1) + N_f$.

(4) If the current cell is stable, the previous one is unstable and, in the driving phase, one grain has fallen on the current cell, the tracer remains in the same cell,
$x^m(k) = x^m(k-1)$,
and its depth is increased by $N_f + 1$,
$d^m(k) = d^m(k-1) + N_f + 1$.

(5) If the current cell is unstable (then N_f grains are moved to the following cell) and no grains have been dropped in the driving phase, then,

i. if the depth of the tracer is less or equal than N_f, $d^m(k-1) \leq N_f$, the tracer moves to the following cell,
$x^m(k) = x^m(k-1) + 1$,
and its depth is initialized with a random value uniformly distributed in $[0, N_f]$,
$d^m(k) = uN_f$.

ii. if the depth of the tracer is greater than N_f, $d^m(k-1) > N_f$, the tracer remains in the same cell,
$x^m(k) = x^m(k-1)$,
and its depth is decreased by N_f,
$d^m(k) = d^m(k-1) - N_f$.

(6) If the current cell is unstable (then N_f grains are moved to the following cell) and one grain has been dropped in the driving phase, then,

i. if the depth of the tracer is less or equal than $N_f - 1$, $d^m(k-1) \leq N_f - 1$, the tracer moves to the following cell,
$x^m(k) = x^m(k-1) + 1$,
and its depth is initialized with a random value uniformly distributed in $[0, N_f]$,
$d^m(k) = uN_f$.

ii. if the depth of the tracer is greater than $N_f - 1$, $d^m(k-1) > N_f - 1$, the tracer remains in the same cell,
$x^m(k) = x^m(k-1)$,
and its depth is decreased by $N_f - 1$,
$d^m(k) = d^m(k-1) - (N_f - 1)$.

II) **Diffusive transport channel**:

(1) If the net diffusive flux in the current cell is negative and larger than the tracer depth,

$D_0 d^2h/dx^2 < -d^m(k-1) < 0$, then the tracer moves to the following cell,
$x^m(k) = x^m(k-1) + 1$,
and its depth is initialized with a random value uniformly distributed in the range $[0, -D_0 d^2h/dx^2]$,
$d^m(k) = -uD_0 d^2h/dx^2$.

(2) In any other case the tracer remains in the same cell,
$x^m(k) = x^m(k-1)$,
and its depth is updated just by adding the corresponding amount of diffusive flux (which can be a positive or negative amount),
$d^m(k) = d^m(k-1) + D_0 d^2h/dx^2$.

That is, only those tracers that are at a depth smaller than N_f from the surface will be moved to the next cell by a passing avalanche. The depth of the tracer at its new location will be randomly chosen in the interval between zero and N_f. The same idea is implemented in the case of the diffusive contribution, but with the relevant depth being now $-D_0 d^2h/dx^2$.

IV. CHARACTERIZATION OF TRACER TRANSPORT IN THE DIFFUSIVE SANDPILE

In this section, we analyze the main properties of tracer transport in the diffusive sandpile. To better understand the analysis it is worth reminding here that the sandpile is naturally split into an "interesting" part where avalanche and diffusive transport coexist, that comprises all cells for $x > x_t$, and a "boring" part that includes all cells $x < x_t$ where only the diffusive channel is active. Here, $x_t = D_0(Z_c - N_f)/P_0$, as we mentioned previously.

A. Global confinement time

From the global point of view, the confinement time of the sand in the sandpile is defined in Eq. (1a) as the ratio of the total mass or amount of sand confined in the sandpile in a steady state, $M = \int_0^L h(x)dx$, to the total external power, $S = P_0 L$. Therefore, once the analytical profiles in steady state and sources are known, the global confinement time can be easily obtained.

$$\tau^{\rm global} = \frac{M}{S} = \frac{\int_0^L h(x)dx}{P_0 L}, \tag{1a}$$

The global confinement time is a function of the parameters that define the sandpile: L, Z_c, N_f, P_0 and D_0. The analytical stationary profiles have been found elsewhere[15,16], both for the case when $x_t \le L$,

$$h(x) = -\frac{P_0 x^2}{2D_0} + Z_a L - \frac{Z_a^2 D_0}{2P_0}, \quad 1 \le x \le x_t < L, \tag{2a}$$

$$h(x) = Z_a (L - x), \qquad x_t \le x \le L, \tag{2b}$$

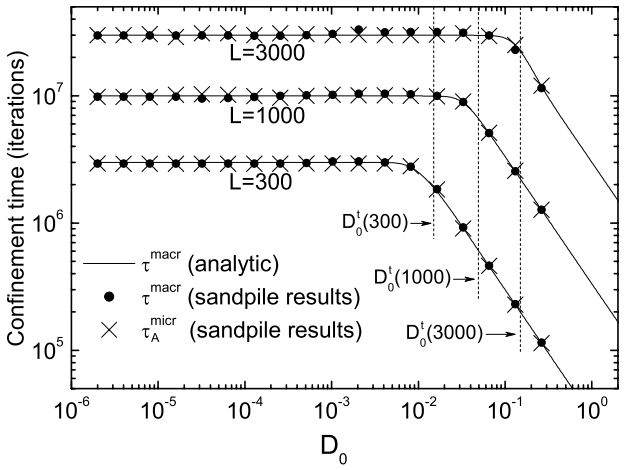

FIG. 3: Tracer confinement times as a function of D_0 for different sandpile lengths. Full lines and filled circles show the analytic values and the numerical estimations for $\tau^{\rm global}$. The parameters used for all sandpile simulations are: $Z_c = 26$, $N_f = 12$ and $P_0 = 10^{-3}$.

and also when $x_t \ge L$,

$$h(x) = -\frac{P_0}{2D_0}\left(x^2 - L^2\right), \qquad 1 \le x \le L. \tag{3}$$

Using Eq.(1a), the corresponding global confinement times are,

$$\tau_{\rm I}^{\rm global} = \frac{Z_a L}{2P_0} - \frac{D_0^2 Z_a^3}{6P_0^3 L}, \quad x_t \le L, \tag{4a}$$

$$\tau_{\rm II}^{\rm global} = \frac{L^2}{3D_0}, \qquad x_t \ge L. \tag{4b}$$

The resulting formulas agree very well with the numerical estimations obtained directly with the diffusive sandpile (see Fig. 3).

B. Tracer particle confinement time

From the particle point of view, however, the confinement time is defined by Eq. (5a) as the average time needed by the tracer to traverse the sandpile ($T_{\rm tr}$), that is also called its **transit time**.

$$\tau^{\rm tracer} = \langle T_{\rm tr} \rangle . \tag{5a}$$

However, the fact that the width of the active strip is always N_f at any cell, as mentioned previously, forces us to initialize tracers at various cells in order to have meaningful statistics. As a result, the distance each tracer needs to travel to traverse the sandpile might be quite different. We have attempted to make later comparisons among different initializations more meaningful by introducing a *normalized* tracer confinement time:

$$\bar{\tau}_n^{\rm tracer} = \frac{L-1}{L - \langle x_0 \rangle} \tau_n^{\rm tracer}, \tag{6}$$

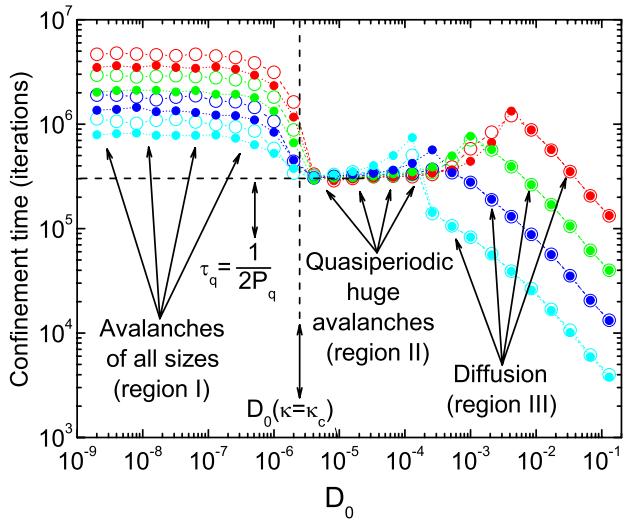

FIG. 4: (Color online) Normalized tracer confinement times as a function of D_0 for different sandpile lengths and initializations: red ($L = 10000$), green ($L = 3000$), blue ($L = 1000$) and cyan ($L = 300$). Hollow symbols stand for initializations of the type I, whilst filled symbols stand for initializations of the type II (see in the text). The parameters in common for all simulations were: $Z_c = 200$, $N_f = 30$ and $P_0 = 10^{-4}$.

where L is the number of cells of the sandpile and $\langle x_0 \rangle$ is the average initial position. Since tracer initializations are made randomly with an uniformly distribution in the range $[x_0^{\min}, x_0^{\max}]$, it follows that $\langle x_0 \rangle = \left(x_0^{\min} + x_0^{\max}\right)/2$.

Fig. 4 shows the normalized confinement times obtained from many simulations as a function of the diffusivity parameter, D_0. Two different types of initialization have been performed in these simulations. Type I initializations are characterized for having $\langle x_0 \rangle = L/20$, while type II have $\langle x_0 \rangle = L/2$. In other words, for type I, particles are initialized within the upper 10% of the cells, and for type II, particles are initialized within the full range of the sandpile, $[1, L]$. The normalized confinement time obtained in each case (represented, respectively, by open and closed circles in Fig. 4) is similar, but not identical.

The first thing to note in Fig. 4 is that, for diffusivities $D_0 < 10^{-6}$ the confinement time is roughly independent of the diffusivity, but scales with the sandpile size. In particular, it can be seen that $\bar{\tau}_B^{\rm micr} \sim L^{0.4}$ in this region which is consistent with the expected value for the non-diffusive sandpile[18], that has been previously found to follow the scaling law $\bar{\tau}_B^{\rm micr} \simeq 0.34 L^{0.4} N_f/P_0$. Transport in this regime exhibits all the classical SOC characteristics: avalanches, self-similarity, memory, and so on, that seem completely unaffected by the presence of finite diffusion.

An abrupt change in scaling is however observed at around $D_0 \sim 10^{-6}$, for the parameters used. The confinement time is suddenly reduced and becomes now completely independent of both diffusivity and system size. Such a dynamical transition of the diffusive sandpile has been known for quite some time[14], and seems to be controlled by the parameter $\kappa = D_0 N_f^2/P_0$, a combination of the drive, diffusion and overturning size. The physical meaning of κ has been related to the average roughness of the sandpile profile, that can be quantified in terms of the variance of the height profile[20]. In our simulations, the change in behaviour takes place at $\kappa_c \sim 22-24$, being completely consistent with the critical value ($\kappa_c = 23$) reported in previous studies[14,16]. It is also worth mentioning that the transition takes place even when the fraction of transport diffusively driven out of the sandpile, $D_0 Z_a$, is still much lower than the integrated source, $P_0 L$.

Transport becomes markedly different above the transition (i.e., for $D_0 > D_0^{\rm II} := D(\kappa_c) = \kappa_c P_0/N_f^2$), being dominated by large quasi-periodic events that have an extent that covers almost completely the "interesting" part of the sandpile. That is, the region $x > x_t$. The frequency of these large events, P_q, can be estimated from balancing the integrated source, $P_0 L$, and the flux leaving the last cell[16]:

$$P_0 L = D_0 Z_a + 2\,(L - x_t)\, N_f P_q. \qquad (7)$$

The first and second terms in the r.h.s. of Eq. (7) represent the contributions of the two transport channels: the diffusive one and the one related to the large, quasi-periodic events. Inserting the analytical expressions for Z_a and x_t, it is found that:

$$P_q = \frac{P_0}{2N_f}\left(\frac{1-(D_0/P_0L)(Z_c - N_f/2)}{1-(D_0/P_0L)(Z_c - N_f)}\right), \qquad (8)$$

that matches very well with the frequency observed in the simulations. In fact, it should be noted that, for $Z_c \gg N_f$, $P_q \approx P_0/2N_f$, which becomes independent of the diffusivity D_0. The average confinement time in this regime seems to be well approximated by $\bar{\tau}_B^{\rm micr} \sim 1/2P_q \sim N_f/P_0$, a simple reflection of the time that tracers will leave the sandpile after a time equal to the lapse from the moment they are added to the sandpile and the next quasi-periodic event.

It is also observed in Fig. 4 that the confinement time starts to increase at the end of the quasi-periodic avalanche region (region II), before decreasing again. The values of D_0 at which both the first increase and late decrease take place both increase with the system size. The explanation for this behaviour is simple. It has to do with the scaling of the transition point, $x_t = D_0(Z_c - N_f)/P_0$, whose value increases with diffusivity. Since we are always initializing the tracers at the same locations, independently of D_0, it happens that, for sufficiently large D_0, a large number of tracers initially fall within the "boring" interior regions, where only the diffusive channel is active. As a result, it takes longer of these particles to reach the "interesting" region that is dominated by the quasi-periodic events. The longer, the larger the sandpile is. Since the confinement time is the sum of the time needed by the tracer to transverse the "boring" or diffusive region, $\bar{\tau}_d^{\rm tracer}$, plus the time needed to traverse the

"interesting" region, $\bar{\tau}_{qp}^{\rm tracer} = N_f/P_0$, the average time needed to exit the sandpile via quasi-periodic events becomes:

$$\bar{\tau}^{\rm tracer} = \bar{\tau}_d^{\rm tracer} + \bar{\tau}_{qp}^{\rm tracer} = \bar{\tau}_d^{\rm tracer} + \frac{N_f}{P_0}. \qquad (9)$$

The last scaling region seen in Fig. 4 (region III) corresponds to the fully diffusive region. That is, when D_0 is sufficiently large so that $x_t \geq L$. Clearly, the value of the diffusivity needed scales linearly with L since it must satisfy:

$$L \sim \frac{D_0^{\rm III}}{P_0}(Z_c - N_f) \rightarrow D_0^{\rm III} = \frac{P_0 L}{Z_c - N_f}. \qquad (10)$$

For $D_0 > D_0^{\rm III}$, transport is completely diffusive. In this region, the confinement time scales: 1) linearly with L, and 2) as $D_0^{-2/3}$, which is different from the expected D_0^{-1} for pure diffusive processes. The reason stems from the treatment of tracer particles we chose: only particles located in the active region of each sandpile's cell are affected by transport mechanisms such as avalanches and/or diffusion, whilst the rest of "regular" particles remain at rest (the pure diffusive scaling would have been recovered if tracked particles were chosen from within the full cell population in the way previously discussed). The discontinuity observed at the beginning of this region comes from the "sudden" disappearance of the "interesting" region, that results in the N_f/P_0 term being dropped from $\bar{\tau}^{\rm tracer}$ in Eq. (9).

C. Probability distribution function of jump-sizes

In order to estimate the probability density function of the sizes of the jumps carried out by the tracer particles, we have considered that a jump starts whenever the tracer changes its position after having been at rest in the preceding iteration. The jump ends when the tracer remains at rest after having been moving in the previous iterations. That is, after the avalanche that carries it has passed. The size of the jump is given by the total number of cells traversed during the avalanche. Fig. 5 shows the jump-size pdfs obtained for simulations with low values of D_0 (region I in Fig. 4) and type I initializations (i.e., in the first 10% of the sandpile cells). These results are in complete agreement with those obtained for the classical running sandpile ($D_0 = 0$), that are characterized by self-similar, critical dynamics[21] (since the tail of the pdfs decay with exponents $p(s) \sim s^{-(1+\alpha)}$ with $0 < \alpha < 1$), that are only limited by the maximum jump size imposed by the finite extension of the sandpile.

Beyond the transition (i.e., for $D_0^{\rm II} < D_0 < D_0^{\rm III}$), the transport dynamics becomes dominated by near system-size, quasi-periodic avalanches involving large amounts of sand that are carried out of the sandpile. Fig. 6(a) shows the pdfs of the jump-sizes obtained for the tracked particles in simulations with values of D_0 within region II

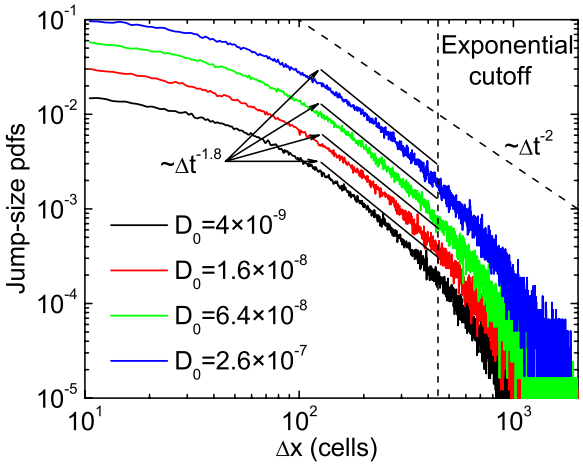

FIG. 5: (Color online) Pdfs for the jump-sizes of the tracked particles as they move across a diffusive sandpile. All values shown for D_0 are within region I in Fig. 4. Other parameters used are: $L = 10000$, $Z_c = 200$, $N_f = 30$ and $P_0 = 10^{-4}$. Power-law fits over the range of interest are also included.

of Fig. 4. Here, parameters are such that x_t ranges from 19 to 7140, covering in a homogeneous way the different possibilities for the value of the transition point. For tracers initialized within the "interesting" region, the shape of the pdf is essentially exponential up to jump-sizes of the order of $L - x_0^{\rm max}$. Then, the pdf becomes flattish (see Fig. 6(b)), ending with a peak at jump size $L - x_t$ (see Fig. 7), and vanishing for larger values. Clearly, all previous traces of self-similarity are now gone.

The explanation for this shape is relatively simple. First, one needs to remember that for cells $x < x_t$ the dynamics is diffusive, whilst for $x > x_t$ the dynamics are governed by large periodic events that empty the active layer in the interval $[x_t, L]$. Any tracer particle initially located at $x_0 > x_t$ will execute a single jump of length $L - x_0$ as it is carried out of the system by a quasi-periodic event. As a result, the distribution of jump sizes will be flat between $L - x_0^{\rm max}$ and $L - x_t$ (i.e., the minimum and maximum allowable values for any jump starting at any $x_0 > x_t$). The peak at jump-size $L - x_t$ is due to the tracer particles that have been initialized instead at $x_0 < x_t$. These particles must first travel diffusively to x_t, and then execute a single jump of size $L - x_t$ when they are eventually transported out of the system by a quasi-periodic event. Clearly, jumps larger than $L - x_t$ are not seen, since quasi-periodic events evacuate the active region too fast for them to become possible. Finally, the exponential distribution observed for jump-sizes up to $L - x_0^{\rm max}$ correspond to the smaller-size avalanches that take place in between periodic events. Their exponential distribution of sizes implies that these avalanches are triggered randomly, a consequence of the continuous smoothing of the profiles carried out by diffusion in between quasi-periodic events, as has been pointed out elsewhere[14].

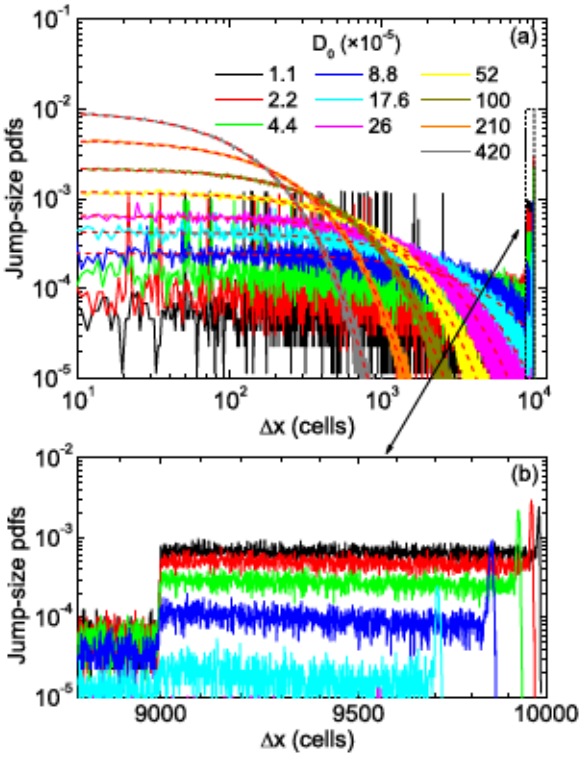

FIG. 6: (Color online) (a) Pdfs for the jump-sizes of the tracked particles as they move across a diffusive sandpile. The dashed region in (a) has been enlarged in (b) to better appreciate the domains 2, 3 and 4 discussed in the text. All values shown for D_0 are within region II in Fig. 4. The rest of the parameters used are the same as in Fig. 5.

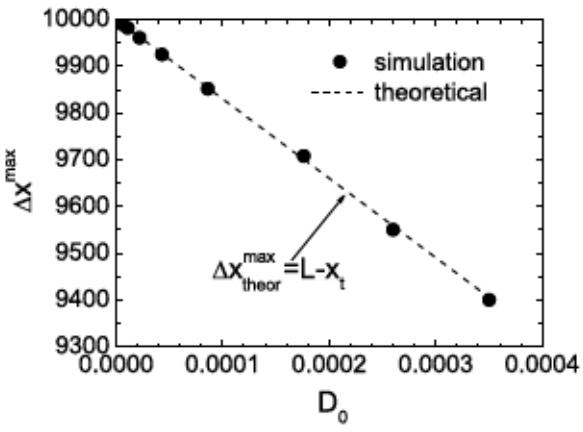

FIG. 7: Position of the last peak in the jump-size pdf (see Fig. 6(b)) as a function of the diffusivity D_0. The dashed line shows the location of $L \quad x_t$, as computed using $x_t = D_0(Z_c \quad N_f)/P_0$.

The exponential behaviour of the jump-size pdfs for sizes below $L - x_0^{\max}$ is well modelled by exponential functions of the type $P(\Delta x) = A\exp(-\Delta x/x_c)$. Here, x_c gives a characteristic scale length for the avalanches that are triggered in between quasi-periodic events. Fig. 8 shows that this length follows an scaling of the type

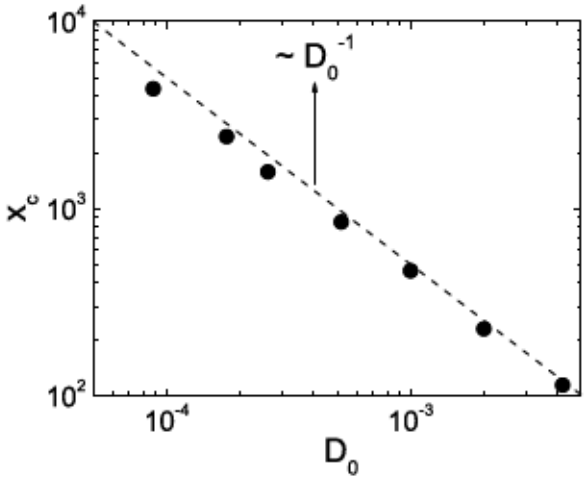

FIG. 8: Characteristic scale length of the tracer jump-size pdfs for sizes less than $L \quad x_0^{\max}$ as a function of the diffusivity parameter D_0.

$x_c \sim D_0^{-1}$. Finally, for $D_0 > D_0^{\rm III}$, both avalanches and quasi-periodic relaxations disappear completely (indeed, since $x_t > L$!) and transport of tracers is purely diffusive across the whole sandpile.

D. Probability distribution function of waiting-times

We proceed now to describe the pdfs that we have obtained for the waiting-times between successive displacements of the tracers. It will be considered that a tracer initiates a waiting-time when it remains at rest having been moved (to its current cell) in the preceding iteration. The waiting-time ends when the tracer moves again to the next cell. Fig. 9 shows the waiting-time pdfs obtained for a selection of the simulations done for $D_0 < D_0^{\rm II}$ (i.e., inside of region I in Fig. 4) and type I initializations, using the same parameters as in the previous section. All the pdfs display extended power-laws with a tail decay roughly given by $p(w) \sim w^{-1.5}$, which are very reminiscent of the pdfs that are obtained for the classical running sandpile (i.e., with $D_0 = 0$). This behaviour is thus indicative of the presence, for $D < D_0^{\rm II}$, of the same kind of self-similar, SOC dynamics that dominates the system in the absence of diffusion. The value of the exponent is also consistent with critical dynamics[21], since it is required that $p(w) \sim w^{-(1+\beta)}$ with $\beta \in (0,1)$. It is worth noting that, in contrast to the jump-size pdfs (see Fig. 5), where the maximum size is limited by the length of the sandpile L, there is no limitation here for the waiting-times. That is the reason for not seeing any exponential cutoffs in waiting-time pdfs.

When the transition to quasi-periodic dynamics takes place (i.e., for $D_0^{\rm II} < D_0 < D_0^{\rm III}$), the waiting-time pdfs no longer exhibit power-law tails, as can be seen in Fig. 10. Instead, there is a well-defined peak at roughly $w_c \sim$

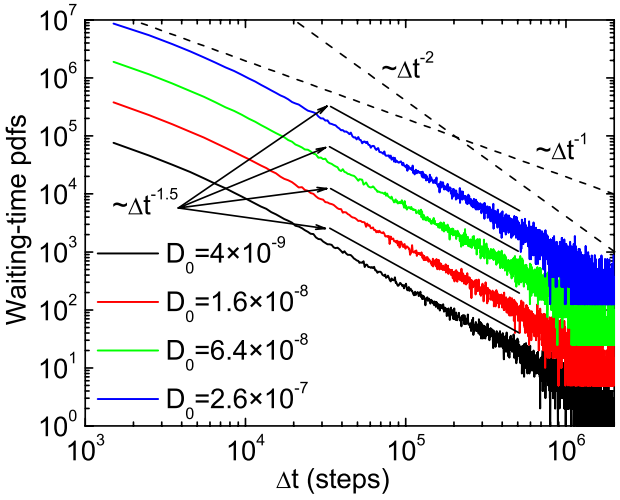

FIG. 9: (Color online) Pdfs for waiting-times of sand particles moving across a diffusive sandpile. All values for D_0 are in the range covered by region I in Fig. 4. The rest of the parameters in common were the same as in Fig. 5. Power-law fits over the range of interest are also included.

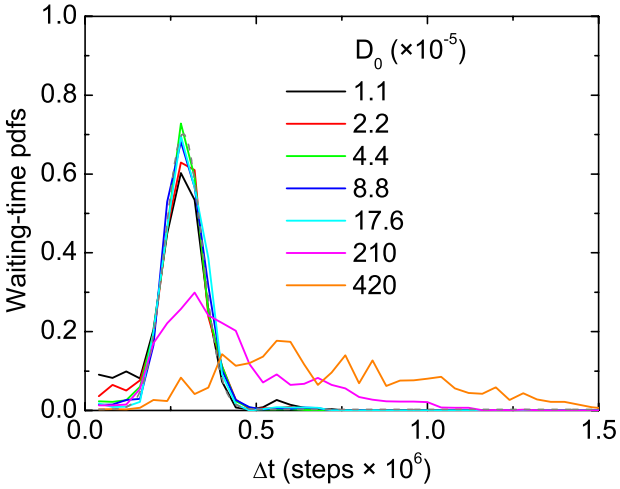

FIG. 10: (Color online) Waiting-time pdfs of sand particles moving across a diffusive sandpile. All values for D_0 are in the range covered by region II in Fig. 4. The rest of the parameters in common were the same as in Fig. 5.

2.9×10^5 that, when fitted to a Gaussian centered at that value, yields a width of about $\sigma \simeq 5.7\times10^4$. It turns out that the location of the peak of the waiting-time pdf is very close to the value $P_q^{-1}/2 \sim N_f/P_0$ (equal to 3×10^5 for the parameters used in the simulations), half of the inverse frequency of the quasi-periodic relaxations. This was to be expected since tracers are transported out of the sandpile whenever one of these events take place, and since they can be added to the system at any time, the average time they have to wait for the next relaxation to take place is half a period.

An interesting new behaviour is observed as D_0 approaches the values that, even if still below $D_0^{\rm III}$, correspond to the points in which the confinement time was seen to ramp up in Fig. 4. It is then observed (see Fig.10) that their waiting-time pdf becomes broader and peaks at increasingly (with D_0) later times than $P_q^{-1}/2$. The reason must be sought in the tracer initialization used that, for all these runs, takes place at values of $x_0 \in [1, x_0^{\rm max}] = [1, 1000] < x_t$, as discussed previously (for $D_0 = 210\times10^{-5} \Longrightarrow x_t = 3570$ and for $D_0 = 420\times10^{-5} \Longrightarrow x_t = 7140$). Since the initial locations of these tracers lie in the "boring" diffusive part of the sandpile, it takes a significant amount of time for them to approach (via diffusion) the $x > x_t$ region that is affected by the quasi-periodic events. Their waiting-times are also more widely distributed (see magenta and orange curves in Fig. 10), due to the different distance from x_t of each tracer, as well as their varying depth within their cells.

V. EFFECTIVE TRANSPORT MODELS

In a recent work[18], we showed that the fractional transport equation given by,

$$\frac{\partial n}{\partial t} = {}_0D_t^{1-\beta}\left[D_{\alpha,\beta}\frac{\partial^{\alpha,1}n}{\partial|x|^{\alpha,1}}\right] + S(x,t), \qquad (11)$$

provides a very good effective model for transport across the active region of the standard (i.e., non-diffusive) running sandpile in its steady state. Here, ${}_0D_t^s$ is a Riemann-Liouville fractional derivative[17] of order $0 < s < 1$ and start-point at $t = 0$, whilst $\partial^{\alpha,1}/\partial|x|^{\alpha,1}$ is the fully asymmetrical, left-sided Riesz-Feller fractional derivative[17,22] of order $0 < \alpha < 1$. $S(x,t)$ is an external source of particles. The two fractional derivatives that appear in Eq. (11) are integro-differential operators that introduce the importance of non-locality and past-history that are characteristic of self-similar dynamics such as SOC into the transport description.

There are different ways to determine the values of the two transport exponents, α and β that better capture the transport dynamics[13,23–25]. Probably, the optimal way is to estimate them by constructing numerically the propagator of Eq. (11). That is, the probability $G(x,t|x',t')$ of finding a particle at location x at time t if it was previously at x' at time t'. Tracers can be easily used for this task simply by considering the temporal evolution of an initially localised population of them. Or the temporal evolution of the distribution of population of tracers that may not be initially localized, but to whose position one subtracts their initial location. Once the propagator is available, one can estimate the values of the exponent α from its asymptotic behavior at fixed time,

$$G(x,t_c|x_0,0) \sim (x-x_0)^{-(1+\alpha)}, \qquad (12)$$

for $x - x_0 \gg D_{\alpha,\beta}^{1/\beta}t_c^{\beta/\alpha}$, and the exponent β from its asymptotic behaviours at fixed position,

$$G(x_c,t|x_0,0) \sim t^{\beta}, \quad \text{for } t \ll D_{\alpha,\beta}^{1/\beta}x_c^{\alpha/\beta}, \qquad (13)$$

and

$$G(x_c, t|x_0, 0) \sim t^{-\beta}, \quad \text{for } t \gg D_{\alpha,\beta}^{1/\beta} x_c^{\alpha/\beta}. \tag{14}$$

In what follows we will used this technique to estimate α and β for the **diffusive** running sandpile for values of D_0 below the transition, being that the only case in which a representation such as Eq. (11) makes any sense. Fig. 11 shows an snapshot (at some fixed time t_c) of the propagators for two different values of $D_0 < D_0^{\rm II}$, together with the standard case $D = 0$.

The snapshots have been displaced vertically on purpose for the sake of clarity. It can be appreciated that all of them scale as $G(x, t_c|x_0, 0) \sim (x - x_0)^{-1.8}$, yielding a value of $\alpha \sim 0.8$. The same behaviour is found for all diffusivities below the transition (i.e., for $D_0 < D_0^{\rm II}$). Analogously, Fig. 12 shows the asymptotic growth and later decay of the propagator at a fixed location, x_c, for the same cases. As can be appreciated, we find a growth that scales approximately as $t^{0.5}$ followed by a decay scaling as $\sim t^{-0.5}$, thus yielding a value of $\beta \sim 0.5$ for all diffusivities below the transition value.

It is interesting to note that the values of the fractional exponents provided by the propagator analysis, $\alpha \sim 0.8$ and $\beta \sim 0.5$ are very close to those that respectively describe the decay of the jump-size and waiting-time pdfs of the tracers, as we discussed in previous sections. This is not a mere coincidence, but completely expected since Eq. (11) can in fact be derived[18] as the asymptotic limit of a fully asymmetric continuous-time random walk[26] defined by a jump-size distribution decaying as $p(s) \sim s^{-(1+\alpha)}$, with $0 < \alpha < 1$, and waiting-time distribution $p(w) \sim w^{-(1+\beta)}$, with $0 < \beta < 1$.

It is however not possible to build an effective model such as Eq. (11) for $D_0^{\rm II} < D_0 < D_0^{\rm III}$, though. The reason must be sought in the complete absence of self-similar

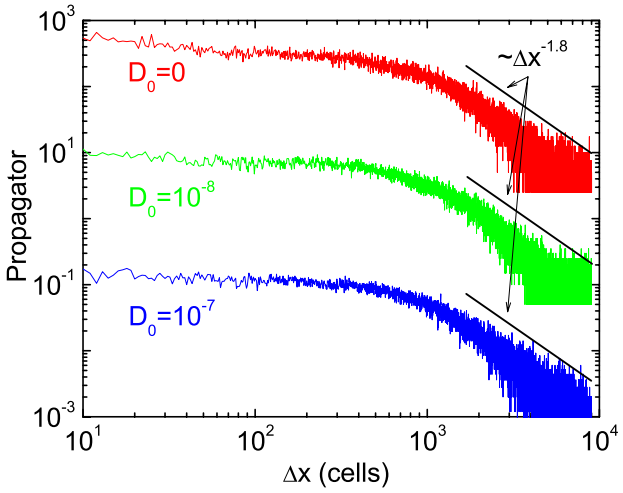

FIG. 11: (Color online) Snapshots of the propagator at some fixed time for three values of the diffusivity below the transition value. The rest of the parameters used were the same as those in the runs shown in Fig. 5.

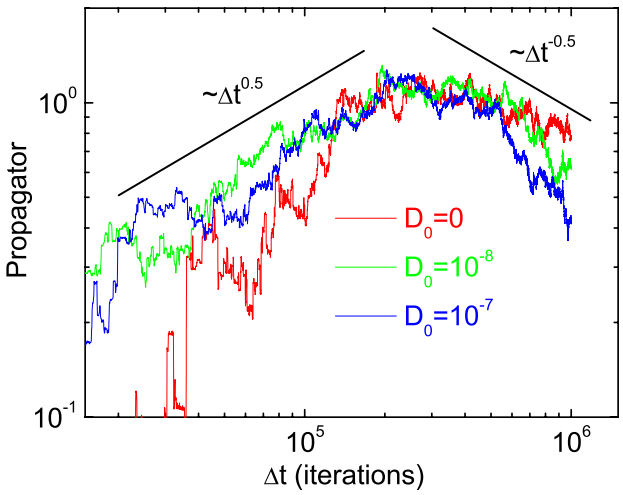

FIG. 12: (Color online) Growth and later decay of the propagator at some fixed location for three values of the diffusivity below the transition value. The rest of the parameters used were the same as those in the runs shown in Fig. 5.

dynamics, with transport being completely dominated by quasi-periodic relaxations with a well defined length scale (roughly, $L - x_t$) and time scale (given by $P_q^{-1}/2$). For $D_0 > D_0^{\rm III}$, the effective transport model is, naturally, the usual classical diffusion equation.

VI. CONCLUSIONS

In this work, we have characterized, by means of a subset of marked grains of sand whose individual trajectories are recorded and analyzed, the three different dynamical transport regimes that take place in the diffusive sandpile as the relative intensity of the diffusive transport channel, with respect to the avalanche-like transport channel, is increased from zero. If all other parameters that define the sandpile are kept fixed, the access to each of the three regimes only depends on the specific value of the diffusivity D_0. If $D_0 < D_0^{\rm II} \simeq \kappa_c P_0/N_f^2$ (with $\kappa_c \simeq 22 - 23$), the dynamics are very reminiscent of the SOC dynamics that govern the sandpile in the absence of diffusion.

In fact, we have shown that an effective transport model similar to the one recently proposed for the non-diffusive sandpile is also valid here. For values of the diffusivity $D_0^{\rm II} < D_0 < D_0^{\rm III} \simeq P_0 L/(Z_c - N_f)$, transport across the sandpile becomes dominated by quasi-periodic events, and all trace of self-similarity is lost. This change of dynamics is perfectly captured by the analysis of the tracer particle trajectories. As a result, effective transport models in terms of fractional derivatives are no longer possible, since transport is now endowed with perfectly defined temporal and spatial scales. Namely, the period between events, P_q^{-1}, and their extension, roughly given by the size of the avalanche region, $L - x_t$. Finally, for $D_0 > D_0^{\rm III}$ the transport dynamics of the sandpile

become diffusive in the traditional sense, being perfectly described by the usual diffusive equation.

Acknowledgments

This research has been sponsored in part by Ministerio de Economía y Competitividad of Spain under Projects No. ENE2015-68265-P and No. ENE2015-66444-R. Research also supported in part by DOE-OFES Grant No. DE-FG02-04ER5741 at University of Alaska. Sandpile simulations have been run in *Uranus*, a supercomputer cluster at Universidad Carlos III de Madrid (Spain) that has been funded by the Spanish Government via the national projects UNC313-4E-2361, ENE2009-12213-C03-03, ENE2012-33219 and ENE2012-31753.

[1] P. Bak, C. Tang and K. Wiesenfeld, *Phys. Rev. Lett.* **59**, 381 (1987).
[2] E. T. Lu and R. J. Hamilton, *Astroph. J.* **380**, L89 (1991).
[3] B. E. Shaw, J. M. Carlson and J. S. Langer, *J. Geoph. Res.* **97**, 479 (1992).
[4] B. Drossel and F. Schwabl, *Phys. Rev. Lett.* **69**, 1629 (1992).
[5] P. Bak and K. Sneppen, *Phys. Rev. Lett.* **71**, 4083 (1993).
[6] S. Mineshige, M. Takeuchi and H. Nishimori, *Astroph. J.* **435**, L125 (1994).
[7] T. Nagatani, *Physica A* **218**, 1 (1995).
[8] S. Field, J. Witt, F. Nori and X. Ling, *Phys. Rev. Lett.* **74**, 1206 (1995).
[9] D.E. Newman, B.A. Carreras, P.H. Diamond and T.S. Hahm, *Phys. Plasmas* **3**, 1858 (1996)
[10] L. P. Kadanoff et al., *Phys. Rev. A* **39**, 6524 (1989).
[11] T. Hwa and M. Kadar, *Phys. Rev. A* **45**, 7002 (1992).
[12] R. Sanchez, D. E. Newman and B. A. Carreras, *Nucl. Fusion* **41**, 247 (2001).
[13] R. Sanchez and D. E. Newman, *Plasma Phys. Contr. Pus.* **57**, 123003 (2015).
[14] D. E. Newman, R. Sanchez, B. A. Carreras and W. Ferenbaugh, *Phys. Rev. Lett.* **88**, 204304 (2002).
[15] R. Sanchez, D. E. Newman, B. A. Carreras, R. Woodard, W. Ferenbaugh and H. R. Hicks, *Nucl. Fusion* **43**, 1031 (2003).
[16] J. A. Mier, R. Sanchez and D. E. Newman, *Phys. Rev. E* **94**, 022128 (2016).
[17] I. Podlubny. *Fractional Differential Equations*. Academic Press, New York (1998).
[18] R. Sanchez, D. E. Newman and J. A. Mier, *Phys. Rev. E* **97**, 052123 (2018).
[19] B. A. Carreras, V. E. Lynch, D. E. Newman and G. M. Zaslaysky, *Phys. Rev. E* **60**, 4770 (1999).
[20] A. Corral and M. Paczuski, *Phys. Rev. Lett.* **83**, 572 (1999).
[21] R. Sanchez and D.E. Newman, "*A primer on complex systems*" (Springer-Verlag, Heidelberg, 2018)
[22] S. G. Samko, A. A. Kilbas and O. I. Marichev. *Fractional Integrals and Derivatives: Theory and Applications*. Gordon and Breach Eds., New York (1993).
[23] R. Metzler and J. Klafter, *Phys. Rep.* **339**, 1 (2000).
[24] D. del-Castillo-Negrete, *Phys. Plasmas* **13**, 082308 (2006).
[25] J.A. Mier, R. Sanchez, L. Garcia, D.E. Newman and B.A. Carreras, *Phys. Rev. Lett.* **101**, 165001 (2008)
[26] E. W. Montroll and G. Weiss, *J. Math. Phys.* **6**, 167 (1965).